Communications in Computational Chemistry
Commun. Comput. Chem., Vol. 7, No. 4, 343–349
doi: 10.4208/cicc.2025.149.01
Regular Article

Unraveling Li-Ion Solvation Dynamics in Ether-Based Electrolytes via High-Throughput Molecular Dynamics Simulations and Machine Learning

Yicheng Gong[1], Weiwei Xie[1,*] and Jun Chen[1,*]

[1]*Frontiers Science Center for New Organic Matter, Haihe Laboratory of Sustainable Chemical Transformations, Key Laboratory of Advanced Energy Materials Chemistry (Ministry of Education), State Key Laboratory of Advanced Chemical Power Sources, College of Chemistry, Nankai University, Tianjin, 300071, China.*

[*] Corresponding authors: xieweiwei@nankai.edu.cn, chenabc@nankai.edu.cn

Received on 29 May 2025; Accepted on 21 June 2025

Abstract: Lithium-ion batteries (LIBs) are now widely used as energy storage systems in portable electronic devices and electric vehicles. The Li-ion solvation dynamics in electrolytes significantly influence the overall performance of LIBs. In this work, we performed high-throughput molecular dynamics smilations on thousands of ether-based electrolytes screened from a vast molecular database containing over 110 million organic molecules. Machine learning models combined with Shapley additive explanation analysis reveal that the presence of bulky alkyl groups reduce the solvent dipole moment, while enhancing the coordination ability of lithium ions with anions. Additionally, the introduction of ether-type groups (-O-) in the rings of cyclic ether molecules negatively affects the solvent dipole moment but positively influences the Li-anion coordination number. In contrast, ether-type groups (-O-) introduced in linear chains correlate positively with solvent dipole moment while negatively with the Li-anion coordination number. This work provides insights into the relation between molecular structure and Li-ion solvation dynamics in electrolyte solutions.

Key words: Li-Ion solvation, machine learning, high-throughput molecular dynamics simulations, electrolyte structure-property relation.

1. Introduction

Lithium-ion batteries (LIBs) have been revolutionized energy storage technology due to their high energy density, lightweight design, and rechargeability. They have dominated the portable-electronic market and showed great promise in large-scale application, such as electric vehicles and smart grids [1-3]. Liquid electrolytes, acting as the 'blood' of LIBs, consist of solvents and lithium salts. Salt ion pairs dissociate in the solvents, with lithium ions surrounded by solvents and/or anions to form lithium-ion solvation sheath. The interactions between cations and solvents [4], cations and anions [5], and anions and solvents [6] determine the solvation environments, leading to the formation of different ion-solvent complexes, such as solvent-separated ion pairs (SSIPs), contact-ion pairs (CIPs) and nano-aggregates (AGGs). These solvation structures significantly influence the overall performance of LIBs [7-11]. For instance, many studies report that LIBs employing weakly-solvated electrolytes, characterized by AGG-dominated solvation structures, outperform those with SSIP-dominated electrolytes under low-temperature and high-voltage conditions [8,9,11,12]. Moreover, AGG-dominated solvation structures promote the formation of inorganic-rich solid electrolyte interphase (SEI), which enhance the stability of lithium-metal batteries [13-15].

Theoretical work has also been conducted to understand elucidate how Li-ion solvation structures affect electrolyte properties

[16-21]. Grossman et. al [16] performed classical molecular dynamics (CMD) simulations to study Li-ion solvation dynamics in various types of electrolyte systems. Rai et. al [17] investigated how Li-ion solvation structures, modulated by salt concentration, impact ion transport in the ethylene carbonate–$LiPF_6$ system. Hamada et al [18]. performed first-principles molecular dynamics simulations on lithium-ion solvation in mixtures of triglyme and lithium bis (trifluoromethylsulfonyl) amide (LiTFSA). It is worth to note that most studies have focused on Li-ion solvation dynamics in a limited number of solvents, which may be insufficient to fully understand the impact of diverse solvation structures on electrolyte properties. In this study, we combined high-throughput MD simulations with machine learning techniques to systematically study the structure-property relationships in ether electrolyte systems.

Recent advances in computational technologies have enabled the integration of machine learning models with high-throughput computation to accelerate the discovery of optimal materials for lithium-ion/metal batteries [22-27]. Compared to traditional experimental trialand-error approaches, computational screening significantly reduces the time required for the material design and experimental validation. For instance, Troyer et al. identified 18 promising solid state electrolytes from 32 million materials using machine learning model combined with high-throughput computation [22]. Their top candidates, $Na_xLi_{3-x}YCl_6$ ($0 \leq x \leq 3$) series, were subsequently synthesized and experimentally validated, demonstrating their high performance. Ma et. al developed a machine-learning workflow to screen fluoroether-based electrolytes for high-stability lithium metal batteries [27].

In this study, approximately 3000 ether molecules were initially selected from the Pub-Chem database, which contains over 100 million organic molecules. Sequent high-throughput MD simulations were carried out to calculate dipole moments and Li-anion/-solvent coordination numbers. Machine learning analysis indicates that alkyl groups correlate negatively with the solvent dipole moment, yet positively correlate with the Li-anion coordination number. Moreover, we find that stronger Li-anion coordination strength corresponds to a lower percentage of SSIPs and a higher percentage of AGGs in the lithium-ion solvation structures. These findings provide valuable insights into the effects of Li-ion solvation structures on electrolyte properties.

2. Molecular dynamics simulations

Molecular dynamics simulations were performed using GROMACS 2023 package [28,29]. Lithium bis (trifluoromethanesulfonyl) imide (LiTFSI) was used as lithium salt. In the high-throughput MD simulations, each electrolyte system contains 600 solvent molecules and the number of LiTFSI molecules was set to mimic 1 mol/L LiTFSI electrolytes. The force field parameters for solvents and ions were derived from the general AMBER force field (GAFF) [30,31], where the atomic charges were generated from restrained fitting on the electrostatic potential (RESP) [32,33] calculated at HF/aug-cc-pVTZ, using Gaussian 16.A.03 software [34]. The atomic charges of ions were scaled down by a factor of 0.7 to account for the neglect of electronic polarization in CMD simulations. After being minimized by the steepest-descent algorithm, the systems were further equilibrated in the NPT ensemble using a thermal annealing approach with a total time of 5 ns. The temperature of systems was initially raised from 0 K to 400 K in a period of 0.5 ns. After being maintained at 400 K for 2 ns, the systems were cooled down to 298 K within 0.5 ns and equilibrated at 298 K for an additional 2 ns. Subsequently, a 20 ns NPT simulation was conducted to sample the structures for data analysis. The temperature was controlled by the V-rescale thermostat with a damping time constant of 0.3 ps, and the pressure was maintained at 1 bar using the C-rescale barostat with a time constant of 2 ps. The cutoffs for the short-range electrostatic and van der Waals interactions were set to 1.2 nm. The calculations of dipole moments, radial density functions (RDFs) and coordination numbers (CNs) of Li-anion/solvent pairs were performed using the post-processing tools implemented in GROMACS software package.

The residence time τ of the $TFSI^-$ anion measures the kinetics of the formation/dissociation of Li^+s solvation structures, which is computed using the Li-anion residence correlation function given by

$$C(t) = \frac{\langle H(t)H(0)\rangle}{\langle H(0)H(0)\rangle},$$

where H denotes the Heaviside function. If the $TFSI^-$ anion reside in the first solvation sheath of Li^+ ion, $H(t) = 1$, otherwise $H(t) = 0$. The cutoff distance defining the first solvation shell of Li^+ is taken as the Li-$TFSI^-$ distance corresponding to the first minimum of the radial distribution function (RDF). The mean residence time τ of the $TFSI^-$ anion was obtained by fitting the exponential function to the residence correlation function.

3. Machine learning methods

The extended connectivity circular fingerprints (ECFPs) [35] implemented in the chemoinformatics toolkit RDKit package [36] was used as molecular descriptor, with each molecule represented as a 2048-dimensional vector. The 2048-dimensional vector of ECFP fingerprints has been reduced to 1353- and 935-dimensional vectors for ring and chain ether molecules, as many fragments do not exist in the ether molecules considered in the present work. Machine learning models, including support vector regression (SVR), random forest (RF), Gaussian process regression (GPR), gradient boosting regression (GBR) and multi-layer perceptron regression (MLP), implemented in scikit-learn package [37] were used to predict the solvent dipole moment and Li-anion coordination number, respectively. Five-fold cross-validation was used for model selection. The mean absolute error (MAE) was employed as the criterion to examine the accuracy of the fitting models. The machine learning model was combined with Shapley additive explanation (SHAP) [38] method to unravel the correlation between the solvent molecular subgroups and targets (i.e., dipole moment, coordination number).

4. Results and discussion

The ether molecules were screened from the public database PubChem, which contains over 110 million organic molecules. To this end, the screening started by considering compounds that only contain carbon, hydrogen and oxygen elements. To this end, the screening started by considering compounds that only contain carbon, hydrogen, and oxygen elements. The compounds with carbonyl groups, hydroxyl groups, and/or unsaturated carbon-carbon bonds were excluded during the screening. The large organic molecules with more than 8 carbon atoms were excluded, as larger ethers often suffer from high viscosity, leading to reduced ionic

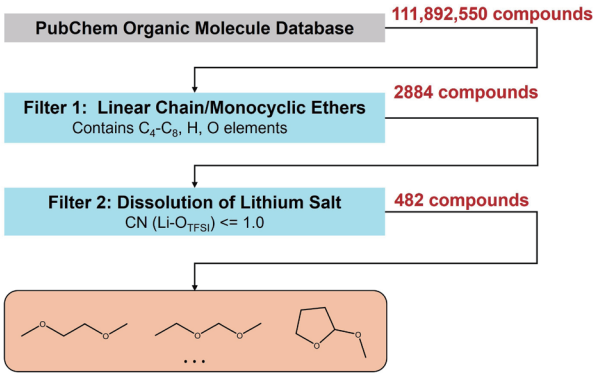

Figure 1. High-throughput screening workflow for ether molecules.

conductivity and thus not appropriate as electrolytes for LIBs. Additionally, the dramatical increasing in molecular diversity with increasing carbon number imposes significant computational challenges that are currently beyond the scope of this study. A total of 2884 compounds fulfilling these initial screening criteria were assessed for the solubility of lithium salt (Filter 1 Figure 1).

A fundamental requirement for an organic molecule to serve as an electrolyte solvent is its ability to dissolve lithium salts. In this study, lithium bis (trifluoromethanesulfonyl) imide (LiTFSI) was employed as the lithium salt. To assess the dissolution of LiTFSI in electrolyte systems, we used the coordination number (CN) of lithium ions with oxygen atoms of $TFSI^-$ anions as a key criterion. Coordination number is a widely used metric to quantify the interactions between lithium ions and solvents or anions. A lower CN (Li-O_{TFSI}) value indicates a stronger coordination strength between lithium ions and solvents, resulting in a higher solubility of lithium salts. Molecular dynamics simulations were conducted on 2884 electrolyte systems with a concentration of 1M LiTFSI. The CN calculations yielded 482 compounds with CN(Li-O_{TFSI}) $\geq$ 1.0 (Filter 2 in Figure 1).

To gain insights into the structure-property relationships of ether-based electrolytes, we trained machine learning models to predict solvent dipole moment (μ_{solv}) and Li-O_{TFSI} coordination number (CN(Li-O_{TFSI})), respectively. Extended connectivity fingerprints (ECFPs), which is widely used in drug design, were employed as the molecular descriptor. Separate models were trained for linear and cyclic ether molecules. Slight variations in mean absolute error was found across the five regression models (see Table S1 and Table S2 in Supporting Information). In the following, the multilayer perceptron (MLP) neural network was used to demonstrate the performance. As shown in Figure 2, the MLP models reasonably reproduce μ_{solv} and CN (Li-O_{TFSI}) obtained by MD simulations.

Next, we combined the Shapley additive explanations (SHAP) approach with the MLP model to study the influence of individual molecular substructures on solvent dipole moment and Li-O_{TFSI} coordination number. Figure 3a-3b present the SHAP values for the top six molecular fragments in linear ether solvents. The ether-type groups (feature 1956, feature 1992, feature 1005, feature

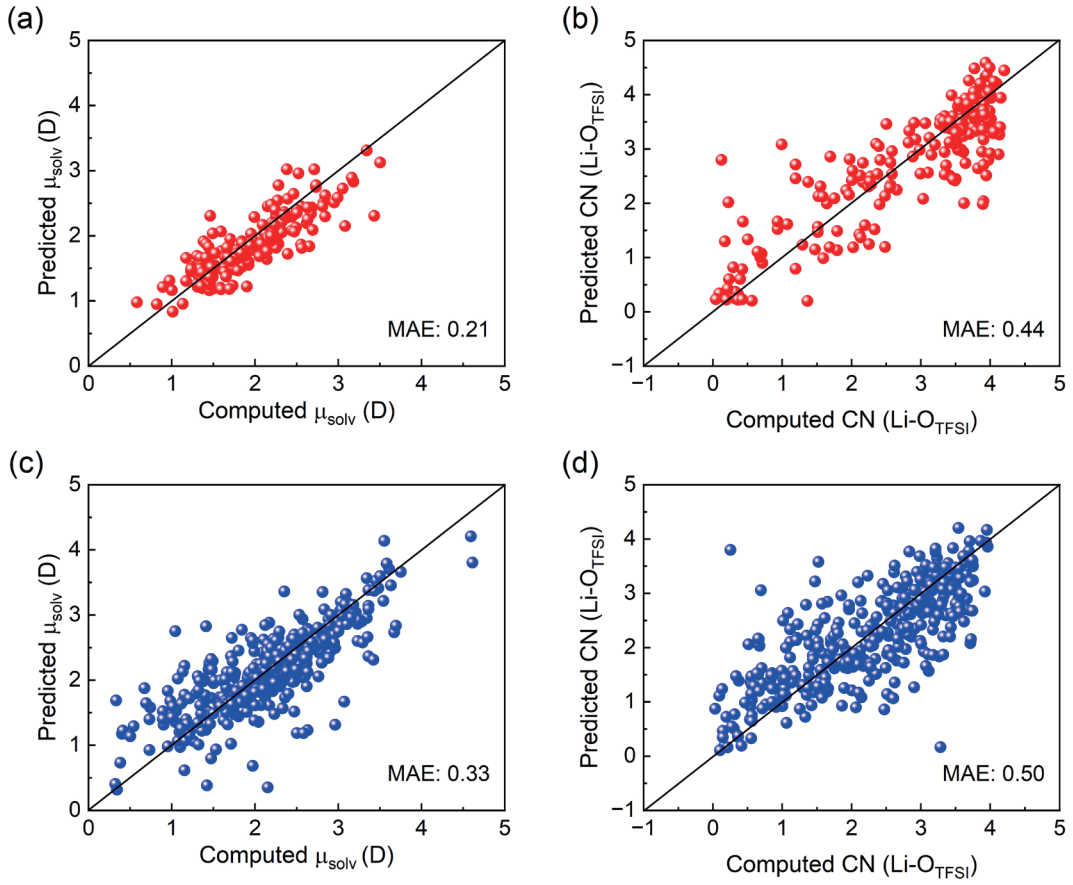

Figure 2. Comparison of the dipole moment(μ) and Li-O_{TFSI} coordination number (CN(Li-O_{TFSI})) predicted by the MLP models against those obtained by molecular dynamics simulations for linear ether electrolytes (a-b) and cyclic ether electrolytes (c-d). The values of mean absolute error (MAE) are shown in figures.

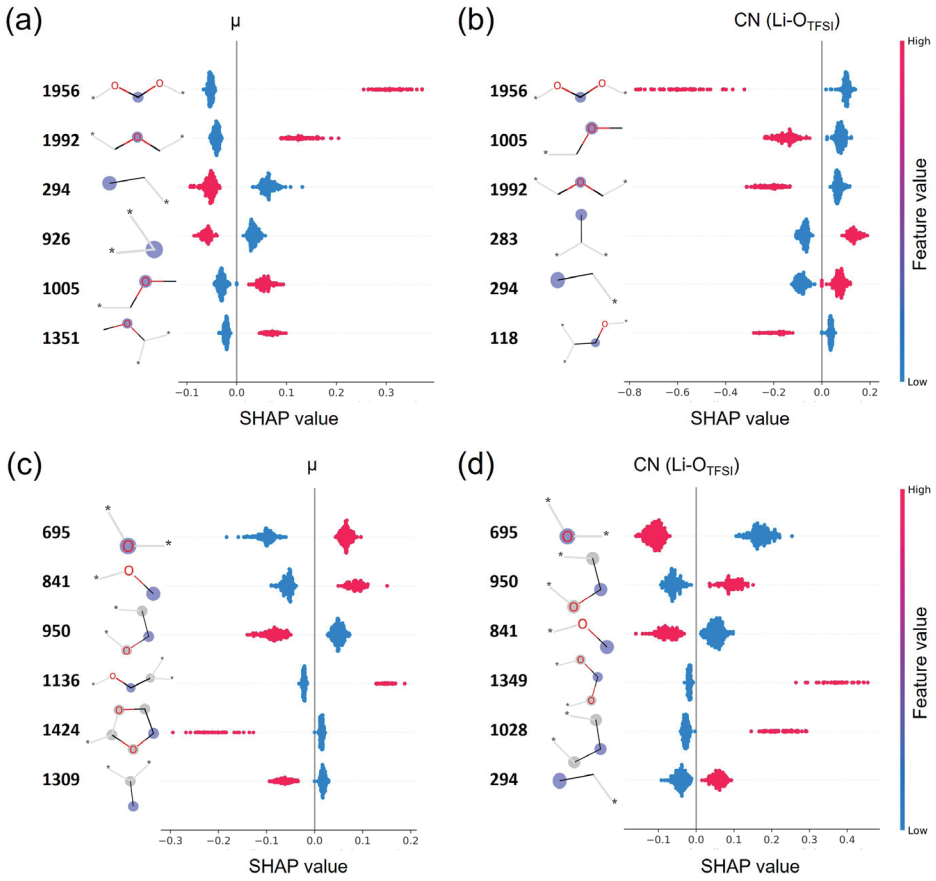

Figure 3. Plots of SHAP values of the top 6 molecular features for the dipole moment(μ) and Li-O$_{TFSI}$ coordination number (CN(Li-O$_{TFSI}$)) for (a-b) linear ether electrolytes and (c-d) cyclic ether electrolytes.

1351) exhibit positive correlations with the dipole moment, while the alkyl groups (feature 294, feature 926) showing negative correlations with the dipole moment. In contrast, the alkyl groups (feature 294, feature 283) show a positive impact on the Li-O$_{TFSI}$ coordination number, while the ether-type groups (feature 1956, feature 1992, feature 1005) exhibit a negative influence on the Li-O$_{TFSI}$ coordination number. These discrepancies can be explained by the different polarity of substituents. Compared with nonpolar alkyl groups, polar ether-type groups increase solvent polarity and thereby enhance lithium coordination ability with solvents, leading to a low Li-O$_{TFSI}$ coordination number. Moreover, solvents containing multiple-ether groups (e.g., feature 1956) tend to form stable multidentate complexes with lithium ions, weakening Li-anion interaction. Conversely, the presence of bulky alkyl groups (e.g., feature 283, feature 294) leads to a high CN(Li-O$_{TFSI}$) value due to the strong steric hinderance to neighboring solvent molecules in Li-ion solvation sheath. Figure 3c-3d presents the SHAP values for the top six molecular features of cyclic ether solvents. Similar to linear ether molecules, the introduction of bulky alkyl groups (feature 1309, feature 1028, feature 294) decrease the solvent

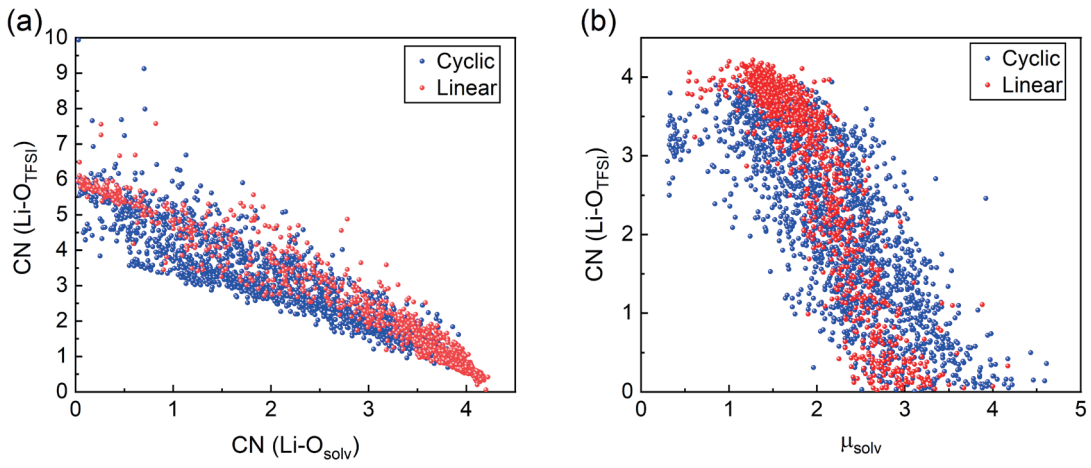

Figure 4. Relationships of the Li-O$_{TFSI}$ coordination number with (a) the Li-O$_{solv}$ coordination number and (b) the solvent dipole moment.

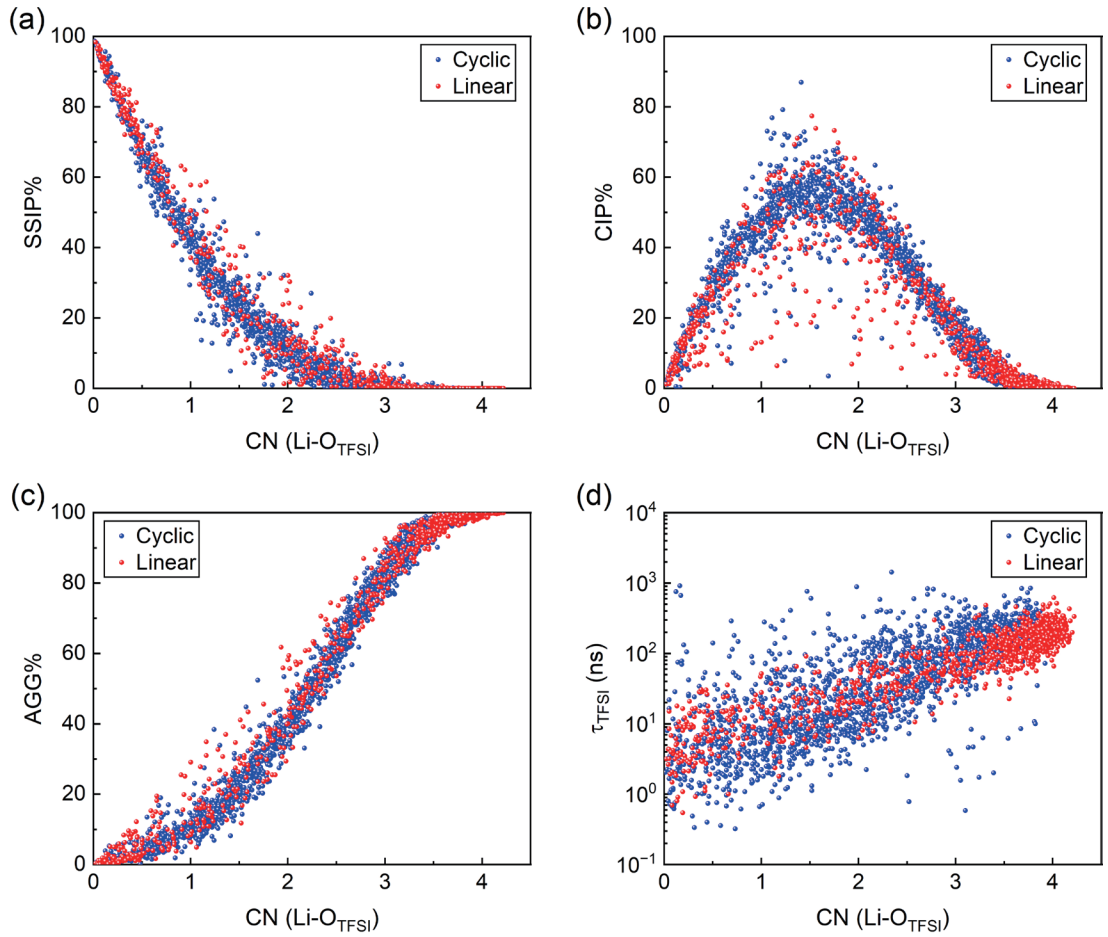

Figure 5. Percentages of (a) SSIPs, (b) CIPs and (c) AGGs in solvation Li-ion structures vs. Li-O_{TFSI} coordination number. (d) Residence time of $TFSI^-$ vs. Li-O_{TFSI} coordination number.

polarity and thus enhance the Li-anion coordination strength. Unexpectedly, the presence of oxygen atoms in the ring structures (features 950, 1424, and 1349) negatively impacts the solvent dipole moment but positively influences the coordination ability of lithium ions with anions. In contrast, the introduction of oxygen atoms in the side chains (features 695 and 841) of cyclic ether molecules shows a positive correlation with the dipole moment but a negative correlation with the Li–O_{TFSI} coordination number. The contrasting effects of ring and linear ether groups can be attributed to their distinct coordination modes with lithium ions. Linear ethers have flexible chains that can form multi-dentate structures with Li^+, enhancing Li-solvent coordination strength and thereby reducing the Li-anion coordination number. In contrast, ring ethers are rigid and exhibit significant steric hindrance. Increasing the number of ether oxygens within the ring does not promote multi-dentate coordination with Li^+; instead, it enlarges the molecular size, which hinders solvent coordination with Li^+ and leads to an increased Li-anion coordination number.

Figure 5a illustrates a negative correlation between the Li-O_{solv} coordination number and the Li-O_{TFSI} coordination number for both linear and cyclic ether molecules. As expected, an increase in the interaction between lithium ions and solvent molecules leads to a decrease in the Li-O_{TFSI} coordination number. Figure 5b shows CN(Li-O_{TFSI}) negatively correlates with the solvent dipole moments, which indicates that solvents with higher polarity exhibit stronger coordination with lithium ions.

In electrolyte systems, lithium ions tend to form ionic complexes with anions and/or solvents. To understand the influence of solvation structures on the coordination ability of lithium ions, we categorized the Li-ion solvation structures into three types: solventseparated ion pairs (SSIPs) where lithium ions are only coordinated with solvents, contaction pairs (CIPs) where only one $TFSI^-$ anion coordinating with lithium ions, and aggregates (AGGs) where two or more $TFSI^-$ anions coordinating with lithium ions. A solvent molecule or $TFSI^-$ anion is considered to be coordinated with the lithium ion only if it is located within a spherical region centered on the lithium ion. The cutoff distance defining the first solvation sheath of Li^+ is taken as the Li^+-solvent/$TFSI^-$ distance corresponding to the first minimum of pair radial distribution function (RDF). Figure 5a-c show the relationships between the Li-O_{TFSI} coordination number and the percentages of SSIPs, CIPs, and AGGs in the Li-ion solvation structures, respectively. The proportion of SSIPs decreases monotonically with increasing Li–O_{TFSI} coordination number, indicating that more anions enter the first solvation sheath of Li ions. The percentage of CIPs initially rises (Figure 5b), reaching a peak around a coordination number of 1.5, and then gradually declines. Conversely, the AGG content decreases monotonically as the Li–O_{TFSI} coordination strength increases. The Li+$TFSI^-$ residence time (τ_{TFSI^-}), defined as the average duration that $TFSI^-$ anions remain in the first solvation sheath of lithium ions, describes the dynamics of Li-ion solvation structures. As shown in Figure 5d, the Li–anion residence time

increases gradually with the increase of the Li-O_{TFSI} coordination number for both linear and cyclic ether molecules. This trend is attributed to the increased participation of $TFSI^-$ anions in lithium ion solvation, which enhances the stability of the Li-ion solvation structures. Note that these findings are transferable to electrolyte systems using other salts (e.g., $LiPF_6$, Figure S1 and Figure S2).

5. Conclusions

In this work, we performed a high-throughput molecular dynamics simulations on 2884 ether electrolyte systems screened from a vast molecular database containing over 100 million organic molecules. The structure-property relationships for the Li-anion coordination number and solvent dipole moment were systematically analysed using machine learning models combined with the SHAP analysis. The results show that the presence of alkyl groups correlate negatively with the dipole moment.These bulky alkyl groups introduce significant steric hindrance to the neighboring solvent molecules in the Li-ion solvation sheath, weakening the Li-solvent interaction and consequently increasing the Li-anion coordination number. Interestingly, the introduction of ether-type groups (-O-) in the rings of cyclic ether molecules negatively impacts the solvent dipole moment but positively influences the Li-anion coordination number. In contrast, ether-type groups (-O-) introduced in the side chains of cyclic ether molecules have a positive effect on the solvent dipole moment while negatively affecting the Li–anion coordination number. These findings provide valuable insights into the solvation dynamics of lithium ions in electrolytes.

Acknowledgments

The authors thank the supports by the National Natural Science Foundation of China (Nos. 22203047, 92472122 and 92372001) and the Fundamental Research Funds for the Central Universities (No. 22JCYBJC00480). The high-throughput MD simulations were performed on Tianhe 3F in National Supercomputer Center in Tianjin.

References

[1] Van Noorden R. A better battery. *Nature*, **507** (2014), 26.

[2] Li M., Lu J., Chen Z., Amine K. 30 years of lithium-ion batteries. *Advanced Materials*, **30** (2018), 1800561.

[3] Lauro S.N., Burrow J.N., Mullins C.B. Restructuring the lithium-ion battery: a perspective on electrode architectures. *eScience*, **3** (2023), 100152.

[4] Shim Y. Computer simulation study of the solvation of lithium ions in ternary mixed carbonate electrolytes: free energetics, dynamics, and ion transport. *Physical Chemistry Chemical Physics*, **20** (2018), 28649-28657.

[5] Osella S., Minoia A., Quarti C., Cornil J., Lazzaroni R., Goffin A.-L., Guillaume M., Beljonne D. Modelling coupled ion motion in electrolyte solutions for lithium sulfur batteries. *Batteries & Supercaps*, **2** (2019), 473-481.

[6] Li K., Subasinghege Don V., Gupta C.S., David R., Kumar R. Effect of anion identity on ion association and dynamics of sodium ions in non aqueous glyme based electrolytes-OTf vs TFSI. *The Journal of Chemical Physics*, **154** (2021), 184505.

[7] Lu D., Li R., Rahman M.M., Yu P., Lv L., Yang S., Huang Y., Sun C., Zhang S., Zhang H., et al. Ligand channel enabled ultrafast Li ion conduction. *Nature*, **627** (2024), 101-107.

[8] Luo L., Chen K., Chen H., Li H., Cao R., Feng X., Chen W., Fang Y., Cao Y. Enabling ultralow temperature (-70 °C) lithium ion batteries: advanced electrolytes utilizing weak- solvation and low-viscosity nitrile cosolvent. *Advanced Materials*, **36** (2024), 2308881.

[9] Liu X., Zhang J., Yun X., Li J., Yu H., Peng L., Xi Z., Wang R., Yang L., Xie W., et al. Anchored weakly solvated electrolytes for high-voltage and low-temperature lithium -ion batteries. *Angewandte Chemie International Edition*, **136** (2024), e202406596.

[10] Wang S., Shi J., Liu Z., Xia Y. Advanced ether-based electrolytes for lithium-ion batteries. *Advanced Energy Materials*, **14** (2024), 2401526.

[11] Holoubek J., Liu H., Wu Z., Yin Y., Xing X., Cai G., Yu S., Zhou H., Pascal T.A., Chen Z., et al. Tailoring electrolyte solvation for Li metal batteries cycled at ultra-low temperature. *Nature Energy*, **6** (2021), 303-313.

[12] Yang Y., Yang W., Yang H., Zhou H. Electrolyte design principles for low temperature lithium-ion batteries. *eScience*, **3** (2023), 100170.

[13] Zhang X.-Q., Chen X., Cheng X.-B., Li B.-Q., Shen X., Yan C., Huang J.-Q., Zhang Q. Highly stable lithium metal batteries enabled by regulating the solvation of lithium ions in nonaqueous electrolytes. *Angewandte Chemie International Edition*, **57** (2018), 5301-5305.

[14] Piao Z., Gao R., Liu Y., Zhou G., Cheng H.-M. A review on regulating Li^+ solvation structures in carbonate electrolytes for lithium metal batteries. *Advanced Materials*, **35** (2023), 2206009.

[15] Yu Z., Rudnicki P.E., Zhang Z., Huang Z., Celik H., Oyakhire S.T., Chen Y., Kong X., Kim S.C., Xiao X., et al. Rational solvent molecule tuning for high performance lithium metal battery electrolytes. *Nature Energy*, **7** (2022), 94-106.

[16] Crabb E., Aggarwal A., Stephens R., Shao Horn Y., Leverick G., Grossman J.C. Electrolyte dependence of Li^+ transport mechanisms in small molecule solvents from classical molecular dynamics. *The Journal of Physical Chemistry B*, **128** (2024), 3427-3441.

[17] Ravikumar B., Mynam M., Rai B. Effect of salt concentration on properties of lithium ion battery electrolytes: a molecular dynamics study. *The Journal of Physical Chemistry C*, **122** (2018), 8173-8181.

[18] Callsen M., Sodeyama K., Futera Z., Tateyama Y., Hamada I. The solvation structure of lithium ions in an ether based electrolyte solution from first-principles molecular dynamics. *The Journal of Physical Chemistry B*, **121** (2017), 180-188.

[19] Kumar N., Seminario J.M. Lithium-ion model behavior in an ethylene carbonate electrolyte using molecular dynamics. *The Journal of Physical Chemistry C*, **120** (2016), 16322-16332.

[20] Yao N., Chen X., Fu Z.-H., Zhang Q. Applying classical, ab initio, and machine learning molecular dynamics simulations to the liquid electrolyte for rechargeable batteries. *Chemical Reviews*, **122** (2022), 10970-11021.

[21] Wan S., Zhao S., Ma W., Chen S. Computational approaches to electrolyte design for advanced lithium-ion batteries. *Chemical Communications*, **61** (39) (2025), 7019-7034.

[22] Chen C., Nguyen D.T., Lee S.J., Baker N.A., Karakoti A.

S., Lauw L., Owen C., Mueller K.T., Bilodeau B.A., Murugesan V., et al. Accelerating computational materials discovery with machine learning and cloud high performance computing: from large scale screening to experimental validation. *Journal of the American Chemical Society*, **146** (2024), 20009-20018.

[23] Cheng L., Assary R.S., Qu X., Jain A., Ong S.P., Rajput N.N., Persson K., Curtiss L.A. Accelerating electrolyte discovery for energy storage with high-throughput screening. *The Journal of Physical Chemistry Letters*, **6** (2015), 283-291.

[24] Guo X., Wang Z., Yang J.-H., Gong X.-G. Machine learning assisted high-throughput discovery of solid-state electrolytes for Li-ion batteries. *Journal of Materials Chemistry A*, **12** (2024), 10124-10136.

[25] Lv C., Zhou X., Zhong L., Yan C., Srinivasan M., Seh Z. W., Liu C., Pan H., Li S., Wen Y., et al. Machine learning: an advanced platform for materials development and state prediction in lithium-ion batteries. *Advanced Materials*, **34** (2022), 2101474.

[26] Allam O., Cho B.W., Kim K.C., Jang S.S. Application of DFT-based machine learning for developing molecular electrode materials in Li-ion batteries. *RSC Advances*, **8** (2018), 39414-39420.

[27] Jia Q., Liu H., Wang X., Tao Q., Zheng L., Li J., Wang W., Liu Z., Gu X., Shen T., et al. Machine learning-driven mass discovery and high throughput screening of fluoroether-based electrolytes for high-stability lithium metal batteries. *Angewandte Chemie International Edition*, **64** (2025), e202424493.

[28] Berendsen H.J., van der Spoel D., van Drunen R. GROMACS: a message passing parallel molecular dynamics implementation. *Computer Physics Communications*, **91** (1995), 43-56.

[29] Abraham M.J., Murtola T., Schulz R., Páll S., Smith J.C., Hess B., Lindahl E. GROMACS: high performance molecular simulations through multi level parallelism from laptops to supercomputers. *SoftwareX*, **1** (2015), 19-25.

[30] Wang J., Wolf R.M., Caldwell J.W., Kollman P.A., Case D. A. Development and testing of a general amber force field. *Journal of Computational Chemistry*, **25** (2004), 1157-1174.

[31] Wang J., Wang W., Kollman P.A., Case D.A. Automatic atom type and bond type perception in molecular mechanical calculations. *Journal of Molecular Graphics and Modellin*g, **25** (2006), 247-260.

[32] Singh U.C., Kollman P.A. An approach to computing electrostatic charges for molecules. *Journal of Computational Chemistry*, **5** (1984), 129-145.

[33] Besler B.H., Merz K.M. Jr, Kollman P.A. Atomic charges derived from semiempirical methods. *Journal of Computational Chemistry*, **11** (1990), 431-439.

[34] Frisch M.J. et al. *Gaussian 16 Revision A.03*, Gaussian Inc., Wallingford CT, 2016.

[35] Rogers D., Hahn M. Extended-connectivity fingerprints. *Journal of Chemical Information and Modeling*, **50** (2010), 742-754.

[36] RDKit. Open source cheminformatics. Available online: https://www.rdkit.org (accessed 28 July 2025).

[37] Pedregosa F., Varoquaux G., Gramfort A., Michel V., Thirion B., Grisel O., Blondel M., Prettenhofer P., Weiss R., Dubourg V., et al. Scikit learn: machine learning in Python. *The Journal of Machine Learning Research*, **12** (2011), 2825-2830.

[38] Lundberg S.M., Lee S.-I. In *Advances in Neural Information Processing Systems 30*, Guyon I., Luxburg U.V., Bengio S., Wallach H., Fergus R., Vishwanathan S., Garnett R. (Eds.), Curran Associates, Inc., 2017, 4765–4774.